European Journal of Pharmaceutical Sciences 118 (2018) 32–39

Contents lists available at ScienceDirect

European Journal of Pharmaceutical Sciences

journal homepage: www.elsevier.com/locate/ejps

The ratiometric fluorescence nanoparticle based on SiRB for pH detection of tumor

Qinghui Wang[a,1], Xiaoyu Ding[a,1], Yuhui Wang[d], Qian Du[a], Tianguo Xu[a], Bin Du[a,b,c,*], Hanchun Yao[a,b,c,*]

[a] School of Pharmaceutical Sciences, Zhengzhou University, Zhengzhou 450001, China
[b] Collaborative Innovation Center of New Drug Research and Safety Evaluation, Henan Province, Zhengzhou 450001, China
[c] Key Laboratory of Targeting Therapy and Diagnosis for Critical Diseases, Henan Province, Zhengzhou 450001, China
[d] The First Affiliated Hospital of Zhengzhou University, Zhengzhou 450001, China

ARTICLE INFO

Keywords:
Tumor microenvironment
Fluorescence imaging
pH detection
Fluorescence switch

ABSTRACT

Tumor pH detection and pH value change monitoring have been of great interest in the field of nanomedicine. In this study, a pH-sensitive near-infrared fluorescence probe SiRB (Si-rhodamine and Boronic acid group) was synthesized by introducing a boronic acid group into the silicon rhodamine structure. ICG (Indocyanine green) as the fluorescence internal standard and SiRB were loaded into PLGA (poly lactic-*co*-glycolic acid) to form PLGA-SiRB-ICG nanoparticle. The experiments showed that the size of the nanoparticle was about 90 nm, which can reach tumor passively by enhancing permeability and retention effect. PLGA in the acidic environment will accelerate the release of cleavage, and the fluorescence ratio of the two probes can reflect the specific pH value in the tumor. The results indicated that the nanoparticle could quantitatively measure the pH value of the tumor site, which is expected to be used in tumor research and treatment.

1. Introduction

Tumor microenvironment is a complex internal environment composed of tumor cells, interstitial cells and extracellular matrix (Gandellini et al., 2015; Hui and Chen, 2015; Wu and Dai, 2017; Alkatout et al., 2017). The characteristics of tumor microenvironment, such as high interstitial fluid pressure, hypoxia, and low extracellular pH, are closely related to the various prognostic factors that control the tumor growth and metastasis (Yang and Yu, 2015; Joyce, 2005). Studies have shown that the tumor acidic environment is caused by anaerobic glycolysis and acidic substance removal disorder (Zhao et al., 2016). Not only would it increase the potential of tumor migration and invasion, but also obstruct the activities of p53 and p-glycoprotein, leading to the MDR (multidrug resistance) in chemotherapy (Florence et al., 2015; Yan and Jurasz, 2016). Therefore, developing a rapid and accurate measurement method of tumor microenvironment pH is conducive to the diagnosis and prognosis of the tumor.

With the development of fluorescent imaging technology and its application in medical imaging, more and more fluorescent probes are synthesized for the detection of small molecule substances. For instance, Wang et al. reported a FRET-based fluorescent polymer dots for the ratiometric imaging of lysosomal HClO in living cells; Chen et al. designed a fluorescent sensor for sensitive and selective detection of copper(II) ion and sulfide anion (Wang et al., 2017; Chen et al., 2016). Among the methods of detecting tumor pH, one way is to connect the fluorophore to the quencher via the hydrazone bonds, which would break in acidic environment to control the fluorescent switch (Li et al., 2017). The drawback of this way is that the hydrazone bonds may rupture during the blood circulation and cause the fluorescence emission before reaching the tumor site. There is also a strategy is adding electron-withdrawing groups to the fluorescent groups, to control the fluorescence emission by PET (photoelectron transfer effect) (Lau et al., 2014). The disadvantages of this strategy are that the sensitivity of the fluorescent switch is low and the electron-withdrawing groups cannot completely inhibit the emission of fluorescence. Moreover, these methods can only compare the level of tumor pH, but cannot measure the specific value of pH. So it is urgently needed to develop an accurate and easy-to-operate method for pH imaging.

As a novel silicon-containing rhodamine derivatives, SiR (Si-rhodamine) has received extensive attention recently. The reason is that SiR has not only excellent photophysical properties and biocompatible properties, but also the excitation and emission wavelengths in the

* Corresponding authors.
E-mail addresses: dubinpaper@sina.com (B. Du), yhchpaper@sina.com (H. Yao).
[1] These authors contributed equally to this work.

https://doi.org/10.1016/j.ejps.2018.03.015
Received 22 November 2017; Received in revised form 6 March 2018; Accepted 14 March 2018
Available online 15 March 2018
0928-0987/

near-infrared region (Tao et al., 2017; Zhu et al., 2015). So it is particularly suitable for tumor tissue imaging. What is more, the spirocyclization of SiR is an attractive strategy for designing NIR (near infrared) fluorescent probes to detect some ions by a reversible ring-opening process (Zhu et al., 2015; Wang et al., 2012). Following this design principle, some SiR-based fluorescent dyes have been exploited for imaging Hg^{2+}, OH^{-1} and the proteins of interest from living cells. As a promising recognition group, boronic acid participates in such an equilibria: in a neutral or mildly basic environment, it binds with the substances containing hydroxyl groups and forms the corresponding boronate which can be reversibly hydrolyzed to boronic acid under acidic conditions (Dervisevic et al., 2017; H.S et al., 2017). Herein we designed and synthesized a SiR-based spirocyclic derivative SiRB (Si-rhodamine and boronic acid), in which a boronic acid group was introduced as a pH-sensitive group. SiRB displayed the reversible H^+-triggered ring-opening process of the corresponding spirocyclic structures accompanied by the remarkable chromogenic and fluorogenic changes. Furthermore, SiRB probe showed the prominent fluorescence changes in the pH range from 7.6 to 5.8, demonstrating an ideal suitability for specific labeling of acidic microenvironment of tumor and tracking the pH changes.

As a biodegradable polymer organic compound, PLGA (poly lactic-*co*-glycolic acid) has good biocompatibility, non-toxicity, good encapsulation and film-forming properties. And it is widely used in pharmaceutical, medical engineering materials and modern industry as a pH-sensitive polymer material (Gu et al., 2015; Guimaraes et al., 2015; Kanamala et al., 2016). In this work, a PLGA-based nanoparticle is fabricated for ratiometric fluorescence imaging and pH detection. It is found that two types of NIR dyes, SiRB and ICG (indocyanine green), can be effectively encapsulated into PLGA via hydrophobic interaction and induce the self-assembly of PLGA to form polymer-dye nanoparticles, with ICG, whose absorbance and fluorescence are inert to pH change, serving as the internal reference item (Kim et al., 2015; Ruhm et al., 2014). The pH-responsive dye SiRB could act as a pH indicator under ratiometric fluorescence imaging. The accurate detection of tumor pH by fluorescence imaging was realized after intravenous injection of this nanoparticle. The gradual acidification of the tumor microenvironment during the tumor growth, as well as the instant tumor pH changes upon injection of external buffers, was vividly observed by this method.

2. Materials and methods

2.1. Materials

3-Bromo-*N*,*N*-dimethylaniline, 2-bromophenylboronic acid (97%), *N*-butyldi ethanolamine (98%) and indocyanine green (ICG) were purchased from Aladdin. poly lactic-*co*-glycolic acid (PLGA, 99%) was obtained from Fu Zhong Pharmaceutical Technology Co., Ltd (Beijing, China). N-Butyl lithium, sec-butyllithium, heptane were obtained from Sigma-Aldrich (St. Louis, Missouri, USA). Tetrahydrofuran (THF), methylene chloride and acetic acid were purchased from Fuyu Fine Chemical Co., Ltd (Tianjin, China). Other reagents were acquired from Sigma-Aldrich. All the reagents were of analytical grade and used without further purification.

2.2. Methods

2.2.1. Synthesis of SiRB

2.2.1.1. Synthesis of 4,4′-methlenebis (3-bromo-N,N-dimethylaniline) (compound 1). A solution of 3-bromo-*N*,*N*-dimethylaniline (25 mmol) in AcOH (80 mL) was added to 37% formaldehyde (125 mmol), and the mixture was stirred at 85 °C for 90 min. After cooling to room temperature, the reaction mixture was carefully neutralized with saturated aqueous $NaHCO_3$ and extracted with CH_2Cl_2 for three times. The organic layer was washed with brine and dried over anhydrous Na_2SO_4. After removal of the solvent under reduced pressure, the residue was purified by silica gel column chromatography with petroleum ether/dichloromethane (2/1, v/v) as eluent. The pure compound 1 was a white solid (yield: 71%).

2.2.1.2. Synthesis of SiX (Si-xanthone). The compound 1 (5 mmol) and anhydrous THF (tetrahydrofuran) (20 mL) were added to a pre-dried flask flushed with nitrogen. The solution was cooled to −78 °C, 1.3 M s-BuLi (sec-butyllithium) (10.7 mL) was added, and the mixture was stirred for 30 min. At the same temperature, a solution of $SiMe_2Cl_2$ (10 mmol) in anhydrous THF (10 mL) was slowly added, and the mixture was slowly warmed to room temperature, then stirred for 3 h. The reaction was quenched by the addition of 2 M hydrochloric acid. Then the mixture was neutralized with $NaHCO_3$ solution, and extracted with CH_2Cl_2. The organic layer was washed with brine and dried over anhydrous Na_2SO_4. The solvent was removed under reduced pressure and the crude was used without further purification. $KMnO_4$ solution (15 mmol) was added to the crude dissolved 50 mL acetone at 0 °C in small portions over a period of 1 h with vigorous stirring. The mixture was stirred for another 1 h at the same temperature, then diluted with CH_2Cl_2 (50 mL), filtered through paper filter and evaporated to dryness. The residue was purified by column chromatography on silica gel to give pure SiX as a yellow solid (yield: 64%).

2.2.1.3. Synthesis of Br-B(2-(2′-bromophenyl)-6-butyl dioxazaborocan). *N*-butyldiethanolamine (20 mmol) was added to a suspension of 2-bromophenylboronic acid (20 mmol) in anhydrous toluene (30 mL). The mixture was heated at 50 °C for 2 h. After cooling to room temperature, the toluene was evaporated under reduced pressure. The remaining clear colorless crude oil was treated with heptane to remove the residual toluene. The resulting suspension was allowed to stand at room temperature overnight. The precipitated solid was collected by filtration, washed with heptane, and dried overnight to give the title compound Br-B as a white solid (yield: 58%).

2.2.1.4. Synthesis of SiRB. To a dried flask flushed with nitrogen, compound Br-B (1.0 mmol) and anhydrous THF (10 mL) were added. The solution was cooled to −78 °C, 1.6 M n-BuLi (n-Butyllithium) (0.75 mL) was added over a period of 10 min and the mixture was stirred for further 20 min. At the same temperature, a solution of SiX (1.0 mmol) in anhydrous THF (10 mL) was slowly added. The mixture was allowed to stir for 20 min at −78 °C, then allowed to warm to room temperature gradually. After stirring for further 1 h, 6 M HCl solution (10 mL) was added and the mixture was stirred for an additional 30 min. The resulting blue solution was neutralized with $NaHCO_3$ solution, and extracted with CH_2Cl_2. The organic layer was washed with brine and dried over anhydrous Na_2SO_4. After removal of the solvent under reduced pressure, the residue was purified by column chromatography on silica gel to give SiRB as a light blue solid (yield: 52%).

2.2.2. Synthesis of PLGA-ICG-SiRB

The PLGA-ICG-SiRB nanocomposites were obtained by self-assembly and subsequently loaded into PLGA nanoparticles. Briefly, 1 mg synthesized SiRB, 0.2 mg ICG and 50 mg PLGA were firstly dispersed in 1 mL acetone. The mixture was added to 40 mg BSA (bovine serum albumin) dispersed in 4 mL deionized water, and stirred overnight in the dark. PLGA-ICG-SiRB nanoparticles were obtained after purification of the suspensions by 8000–12,000 D dialysis bag.

2.2.3. Characterization of PLGA-ICG-SiRB

The PLGA-ICG-SiRB nanoparticles were characterized by transmission electron microscopy (TEM, Tecnai G2 20, FEI, USA). UV–vis absorption spectra were recorded using a UV–vis spectrometer (Lambda 35, Perkinelmer, USA). Fluorescence spectra were recorded with a RF-

5301 fluorospectrophotometer (Shimadzu, Japan). The hydrodynamic diameters of the obtained nanoparticles were determined by a dynamic light scatter (DLS, Zetasizer Nano ZS-90, Malvern, England).

2.2.4. Cellular experiments of PLGA-ICG-SiRB

MCF-7 human breast cancer cell line was gained from Chinese Academy of Sciences Cell Bank (Catalog No. HYC3204, Beijing, China). Cells were cultured in DMEM with 10% FBS and 1% penicillin/streptomycin in 5% CO_2 and 95% air at 37 °C in a humidified incubator.

To assess the cancer cell toxicity of the PLGA-ICG-SiRB nanoparticles. MCF-7 cells were incubated with fresh medium containing various concentrations of PLGA-ICG-SiRB, PLGA, ICG and SiRB for 24 h. Finally, the cell viability assay was determined using SRB (sulforhodamine B).

2.2.5. Imaging experiment and pH detection

All animal experiments were performed under a protocol approved by Henan laboratory animal center. The Life Science Ethics Committee (Zhengzhou University) reviewed and approved the entire animal protocol prior to initiation of the experiments. Mice tumor models were generated by subcutaneous injection of 1×10^6 S180 cells in 0.1 mL saline into the right shoulder of Kunming mice (18–22 g). When the tumor reached a mean size of about 100 mm^3 (~6 days after tumor inoculation), the mice were intravenously injected with PLGA-ICG-SiRB (200 μL per mouse). Fluorescence imaging of mice was performed at preset times by in vivo imaging system (Bruker, Germany) equipped with Kodak in Vivo Imaging System FX PRO (Carestream Health, Inc., USA). For fluorescence imaging, according to the UV–vis absorption spectra obtained under 2.2.3 above, the entire tumor area was exposed to the light (630 nm and 780 nm). The fluorescence images were captured at 650 nm and 830 nm emission wavelengths. The I_{650}/I_{830} fluorescence signal ratios were calculated by the software and could be used to measure the pH values in the tumor.

3. Results

3.1. Synthesis and characterization of pH-sensitive NIR fluorescent probe SiRB

SiRB was synthesized through a four-step method and its properties were investigated. First, SiX was prepared by two-step reaction with 3-bromo-*N*,*N*-dimethylaniline as a raw material. Then, the probe SiRB

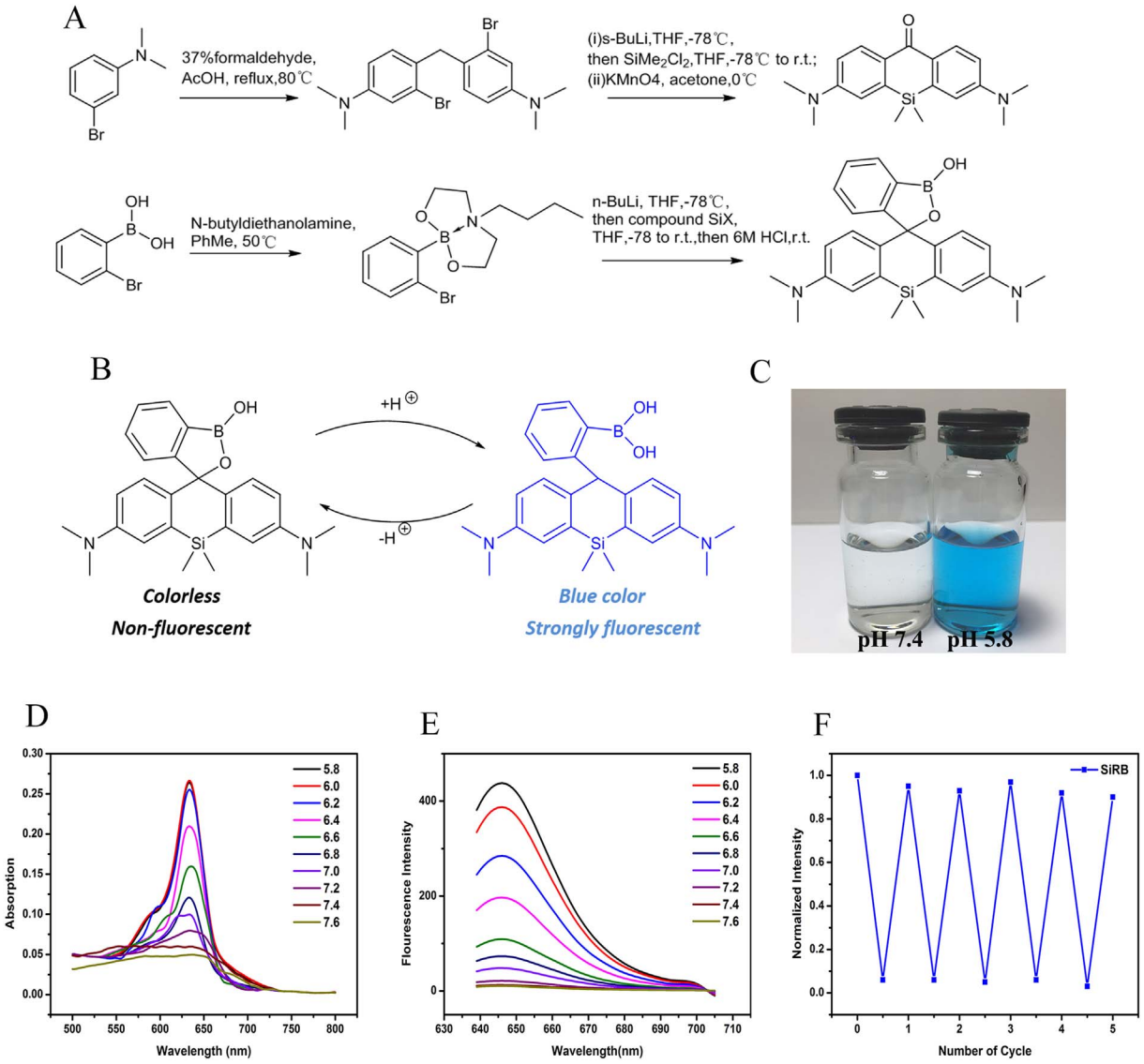

Fig. 1. Synthesis and characterization of SiRB. (A) Synthesis of SiRB; (B) chemical structures of SiRB and the reversible transformation between boronate and boronic acid; (C) the color changes of SiRB in different pH PBS solution (containing 1% DMSO); (D) UV–Vis absorbance spectra recorded in buffers with different pH values; (E) fluorescence spectra of SiRB recorded in buffers with different pH values under 630 nm excitation; (F) the reversible fluorescence responses of SiRB (changes in the fluorescence at 647 nm between pH 7.6 and 5.8).

was prepared by addition of a lithiated benzene moiety bearing a protected boronic acid group to SiX, followed by deprotection in hydrochloric acid solution. In the protection of the boronic acid group, N-butyl diethanolamine was chosen as a protective reagent because of its tolerance to lithiation and effective deprotection (Fig. 1A) (Uno et al., 2014). The structures of synthetic intermediates and SiRB were confirmed by ^{1}HNMR spectroscopy (Fig. S1, Supporting information). The H^+-dependent color response of SiRB in PBS (phosphate buffer saline) (containing 1% DMSO, dimethyl sulphoxide) was observed (Fig. 1B, C). When the pH value of the solution was 7.4, the solution was colorless and non-fluorescent. However, when the pH value was 5.8, the color of the solution became light blue to give strong fluorescence.

To examine the spectral profile of SiRB, we measured the UV–Vis absorption spectra and fluorescence emission spectra of SiRB in PBS at different pH values. With the decrease of pH values range from 7.6 to 5.8, the simultaneous enhancements in UV–Vis absorption at 630 nm and fluorescence intensity at 647 nm were noticed (Fig. 1D, E). The UV–Vis absorption and fluorescence intensity of SiRB increased by 5.3 and 41 times range from pH 7.6 to 5.8, respectively. In order to further study the mechanism of SiRB fluorescence switch, we conducted a fluorescence switch reversibility experiment (Fig. 1F). After five cycles, no noticeable changes in the emission were observed in SiRB. Meanwhile, the color of probe SiRB changed repeatedly between colorless and blue.

3.2. Synthesis and characterization of PLGA-ICG-SiRB

The PLGA-ICG-SiRB nanoparticle was synthesized and its properties were investigated. We prepared the PLGA-ICG-SiRB by the method of solvent emulsification and volatilization. The SiRB and ICG fluorescent probes were encapsulated in PLGA polymers to form core-shell nanoparticle. The hydrodynamic diameter and apparent zeta potential of PLGA-ICG-SiRB were measured by DLS (Figure, 2A, B). The average particle size of PLGA-ICG-SiRB was 95.13 ± 0.21 nm and the average zeta potential of PLGA-ICG-SiRB was −8.14 ± 0.13 mV. We observed the morphology of the probe PLGA-ICG-SiRB by TEM (Fig. 2C). From the figure of TEM, we can see the probes were packaged in PLGA to form a core-shell structure and the whole preparation presented a spherical morphology. Under pH 5.8, UV–Vis absorbance spectra of different dye-loaded nanoparticles were measured (Fig. 2D), the results suggested that PLGA-ICG-SiRB showed the characteristic peaks of both ICG and SiRB were located at 780 nm and 630 nm, respectively. The fluorescence spectra of ICG, PLGA-SiRB, PLGA-ICG and PLGA-SiRB-ICG were also compared at pH 5.8 (Fig. 2E). As shown in Fig. 2F, the absorptions of ICG (780 nm) remained almost unchanged as the variation of the pH values. However, the maximum UV–Vis absorptions of SiRB at 630 nm still significantly increased with decreasing pH. The ratio of the maximum absorption of the two probes decreased with the increase of pH values (Fig. 2G).

The time-dependent releases of SiRB and ICG from PLGA-ICG-SiRB were measured across two pH values, 5.8 and 7.4 (Fig. 2H), which represents the tumor acidic microenvironment and human normal blood circulation pH value, respectively. As we can see from Fig. 2H, the release rates of ICG and SiRB at pH 5.8 were significantly higher than those at pH 7.4 in the serum solution in 60 h. In the acidic environment, the cumulative release rates of SiRB and ICG probes were 68% and 76%, respectively. However, in the neutral environment, the cumulative release rates were only 9% and 11%.

The PLGA-ICG-SiRB nanoparticles also showed great stability in different physiological solutions. First, we tested the stability of PLGA-ICG-SiRB in serum solutions (pH 7.4). The results showed that the nanoparticle in neutral serum solution behaved no significant change in particle size in one week (Fig. 3A). To see if the salt substances in vivo can affect the stability of PLGA-ICG-SiRB, we also added 20 mM NaCl, KCl, $CaCl_2$ to the serum solutions to imitate the human physiological environment. The results showed that the UV–Vis absorption spectra of PLGA-ICG-SiRB did not change obviously with the addition of salts at pH 7.4 and 5.8 (Fig. 3B, C).

3.3. Cell experiment

We used breast cancer cell MCF-7 as a model cell for cell experiments. It was essential the cytotoxicity of the prepared nanoparticle as fluorescence imaging reagent. Thus, the cytotoxicity of PLGA-ICG-SiRB in vitro was evaluated by the SRB method (Fig. 4A). Under the SiRB concentration (20 μM), none of the four groups showed significant cytotoxicity. On the other side, when the concentration was higher than 20 μM, the cell viability declined slimly as the concentrations of PLGA-ICG-SiRB, PLGA, ICG, SiRB increased. At the same concentration, the cytotoxicity of ICG and SiRB was higher than that of PLGA and PLGA-ICG-SiRB upon 40 μM, indicating that PLGA had almost no cytotoxicity at normal dosing levels. The encapsulation of ICG and SiRB into PLGA could effectively reduce the cytotoxicity of the probes.

From the laser confocal fluorescence microscopy experiment (Fig. 4B–E), we have also surprisingly found that our synthetic fluorescent probe, SiRB, not only entered tumor cells, but also targeted lysosomes in tumor cells. We stained MCF-7 cells with DAPI (4′,6-diamidino-2-phenylindole), LysoTracker Green DND-26 (commercially available lysosome-specific probe) and SiRB. After 6 h staining, the extra dyes would be washed and the cells were observed under laser confocal fluorescence microscopy. DAPI could enter the nucleus and emit blue fluorescence (Fig. 4B). LysoTracker Green DND-26 entered the lysosome of the cell and releases green fluorescence (Fig. 4C). The picture (Fig. 4D) showed the fluorescence emission of SiRB in cells and Fig. 4E was the merged image. The experimental results showed that the staining of probe SiRB fited well with that of LysoTracker Green DND-26.

3.4. Imaging experiment and pH detection

Fluorescence imaging and pH detection of tumor was carried out by recording the fluorescent signals of both SiRB and ICG from PLGA-ICG-SiRB dispersed in serum solution with different pH values (Fig. 5A). The fluorescent signals at 650 nm (emission peak of SiRB) exhibited an obvious decrease as the increased pH value in the range of 5.8–7.6, while the signals at 830 nm (emission peak of ICG) hardly changed (Fig. 5B). The fluorescence intensity ratios between 650 nm and 830 nm (650/830) also exhibited a sharp decrease in that range as the increase of pH values (Fig. 5C). We performed linear regression calculations based on the data in Fig. 5C. By calculation, we got the linear regression equation: $Y = 1.2X + 9.19$, and the linear regression coefficient R^2 was 0.9653. Due to the high linearity, it is shown that there is a linear relationship between the fluorescence ratio and the pH value in the measured pH range. We can use this linear regression equation to estimate the approximate pH values of tumor tissue and other major organs.

We calculated the pH of tumor tissue and different organs by this method. We constructed ascites tumor S180 into Kunming mice to construct tumor-bearing mice animal model. To compare the differences in pH values between tumor and other major organs and illuminate the distribution of probes in different organs, ex vivo imaging of major organs as well as tumors collected from mice at 6 h after *i.v.* injection of PLGA-ICG-SiRB were conducted (Fig. 5D). As we can see from Fig. 5E, the fluorescence intensity of the two probes at the tumor site was significantly higher than that of other organs. The results of Fig. 5F showed the relationship between the fluorescence ratio of the two probes and the pH values. The data in the graphs were taken into the linear regression equation to calculate the pH of the tumor site and the value was 6.57. The pH of the remaining organs was approximately 7.45. We also calculated the changes in tumor pH values for different growth days by this method (Fig. 5G). The results showed that with the increase of the number of days of tumor growth, the fluorescence ratio

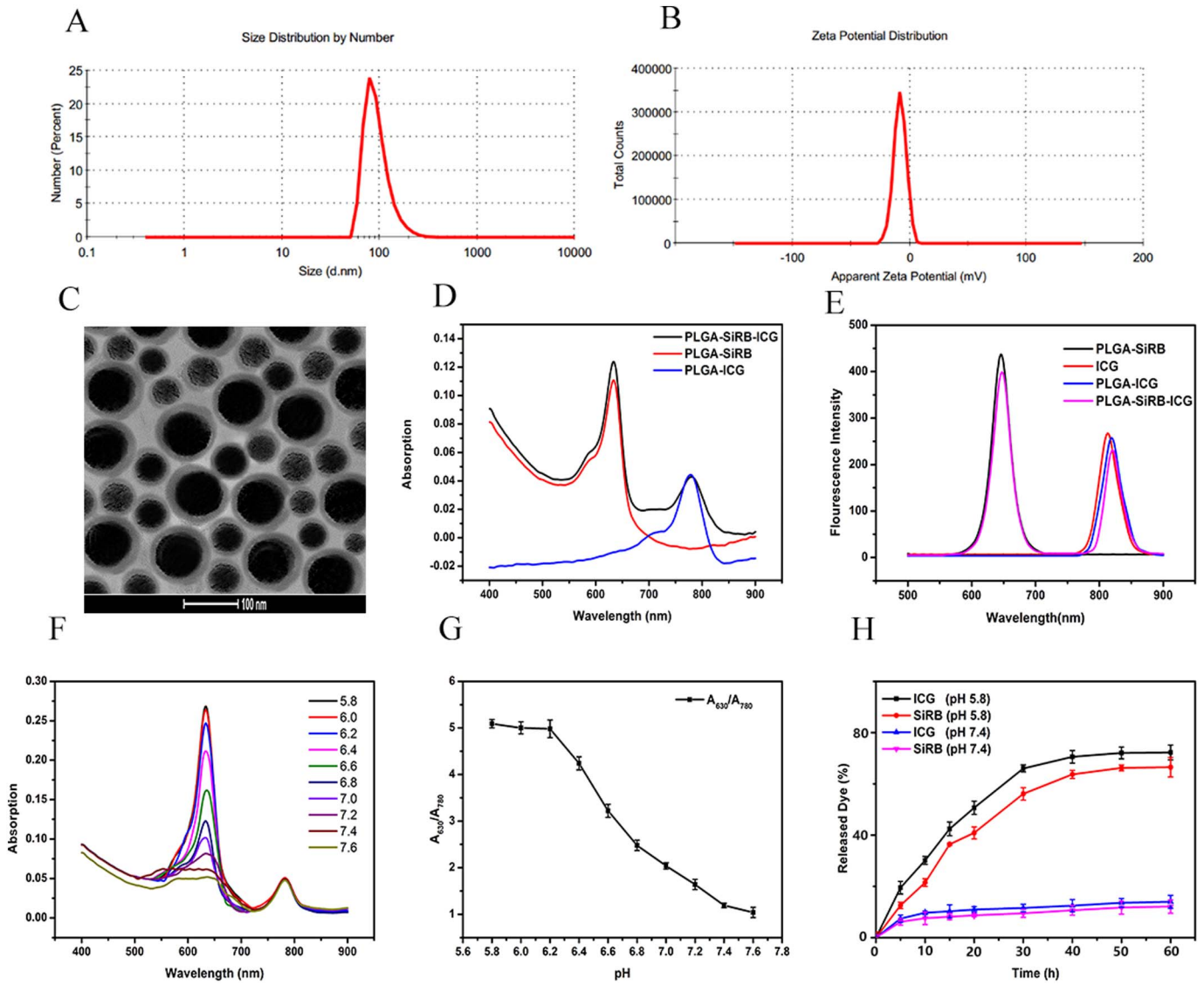

Fig. 2. Characterization of PLGA-SiRB-ICG. (A) and (B) DLS analysis results of PLGA-ICG-SiRB; (C) TEM images of PLGA-ICG-SiRB; (D) UV–Vis absorbance spectra of PLGA-ICG-SiRB; PLGA-SiRB and PLGA-ICG; (E) fluorescence spectra of PLGA-SiRB, ICG, PLGA-ICG and PLGA-SiRB-ICG; (F) UV–Vis absorbance spectra of PLGA-ICG-SiRB recorded in buffer solutions at different pH values; (G) the absorption ratio A_{630}/A_{780} of PLGA-ICG-SiRB dispersed in buffers with different pH values; (H) The time-dependent release of SiRB and ICG from the PLGA-ICG-SiRB nanoparticles in serum solution at pH 7.4 and 5.8.

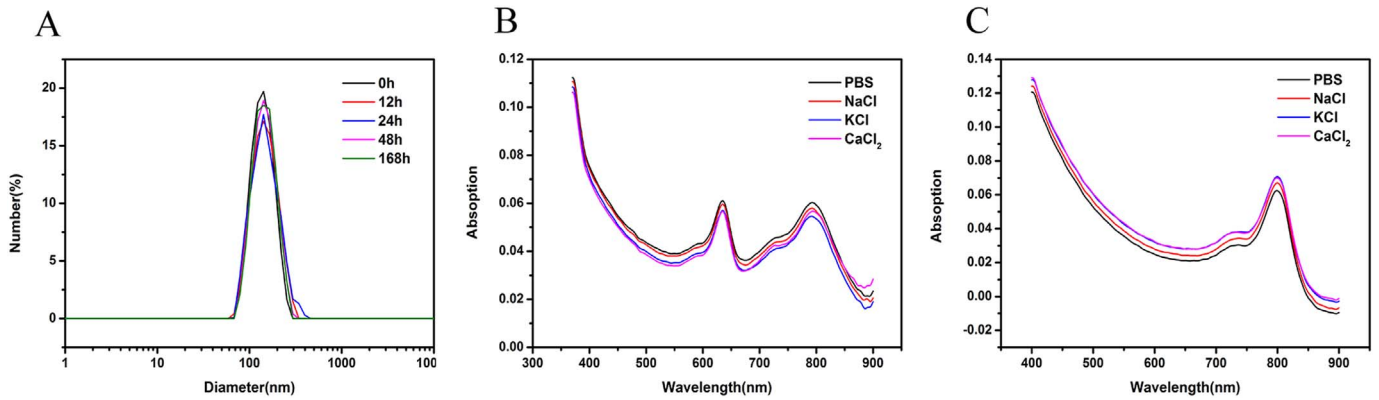

Fig. 3. Stability of PLGA-ICG-SiRB nanoparticles. (A) DLS data of PLGA-ICG-SiRB dispersed in serum solution (pH 7.4) for different periods of time; (B) and (C) The absorption spectra of PLGA-ICG-SiRB dispersed in pH 5.8 or 7.4 PBS (add 1% DMSO) with 20 mM NaCl, KCl or $CaCl_2$.

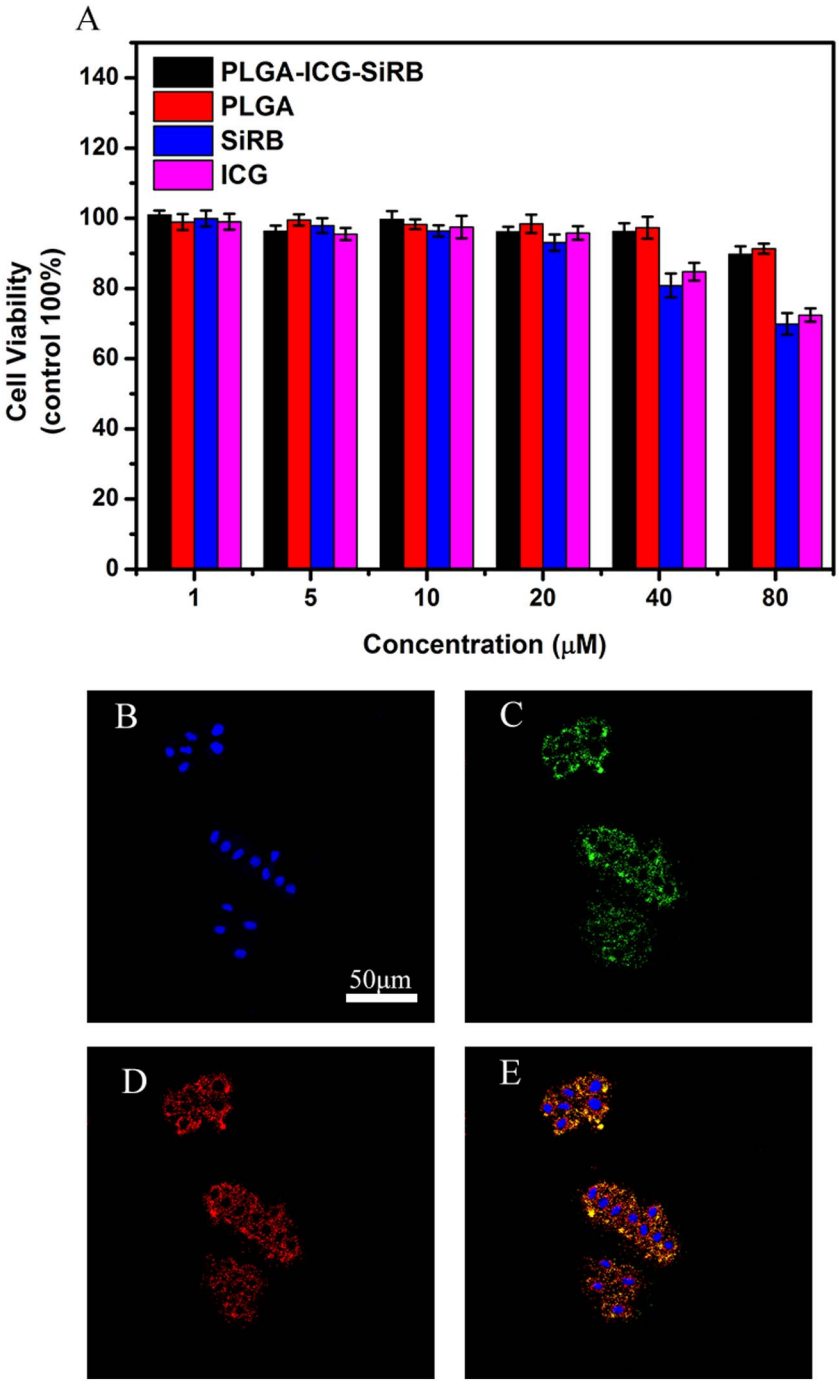

Fig. 4. Cellular experiment of the PLGA-ICG-SiRB nanoparticles. (A) Cell viability of MCF-7 cells at different concentrations of SiRB contained in the PLGA-ICG-SiRB nanoparticles after 24 h incubation; (B–E) Fluorescence images of MCF-7 cells incubated with PLGA-ICG-SiRB nanoparticles for 6 h (blue: cell nuclei stained by DAPI, green: lysosome stained by LysoTracker Green DND-26, red: cell stained by PLGA-ICG-SiRB). (For interpretation of the references to color in this figure legend, the reader is referred to the web version of this article.)

was also increasing, and the pH value of tumor microenvironment was decreasing. The pH values of tumor site from 7 days to 19 days were 6.83, 6.60, 6.38, 6.19 and 6.01, respectively. This finding has the potential to be used in defining tumor stages and detecting tumor progression.

4. Discussion

In this paper, we successfully synthesized and characterized the near-infrared fluorescence probe SiRB, which has a sensitive response at pH 5.8–7.6. SiRB formed a colorless solution and no fluorescence was emitted in a neutral buffer solution, but underwent a reversible light blue color change in acidic environment. These phenomena implied that the boron-containing probe SiRB was sensitive to H^+, and the reversible color change was likely to be induced by the reversible ring-opening process of the corresponding rings (Lukinavicius et al., 2013).

Based on the probe SiRB, we prepared the PLGA-ICG-SiRB nanoparticle which can be used to accurately reflect the pH value of tumor and other organs by fluorescence ratio imaging. The ring opening process of the borate-based spiro-rings in the SiRB dye as the decrease of pH, would lead to enhance the absorption of SiRB, as well as increased fluorescence emission. On the other hand, the fluorescence of ICG, different from that of SiRB, is inert to pH changes. So ICG may serve as the internal reference when SiRB is used for pH sensing.

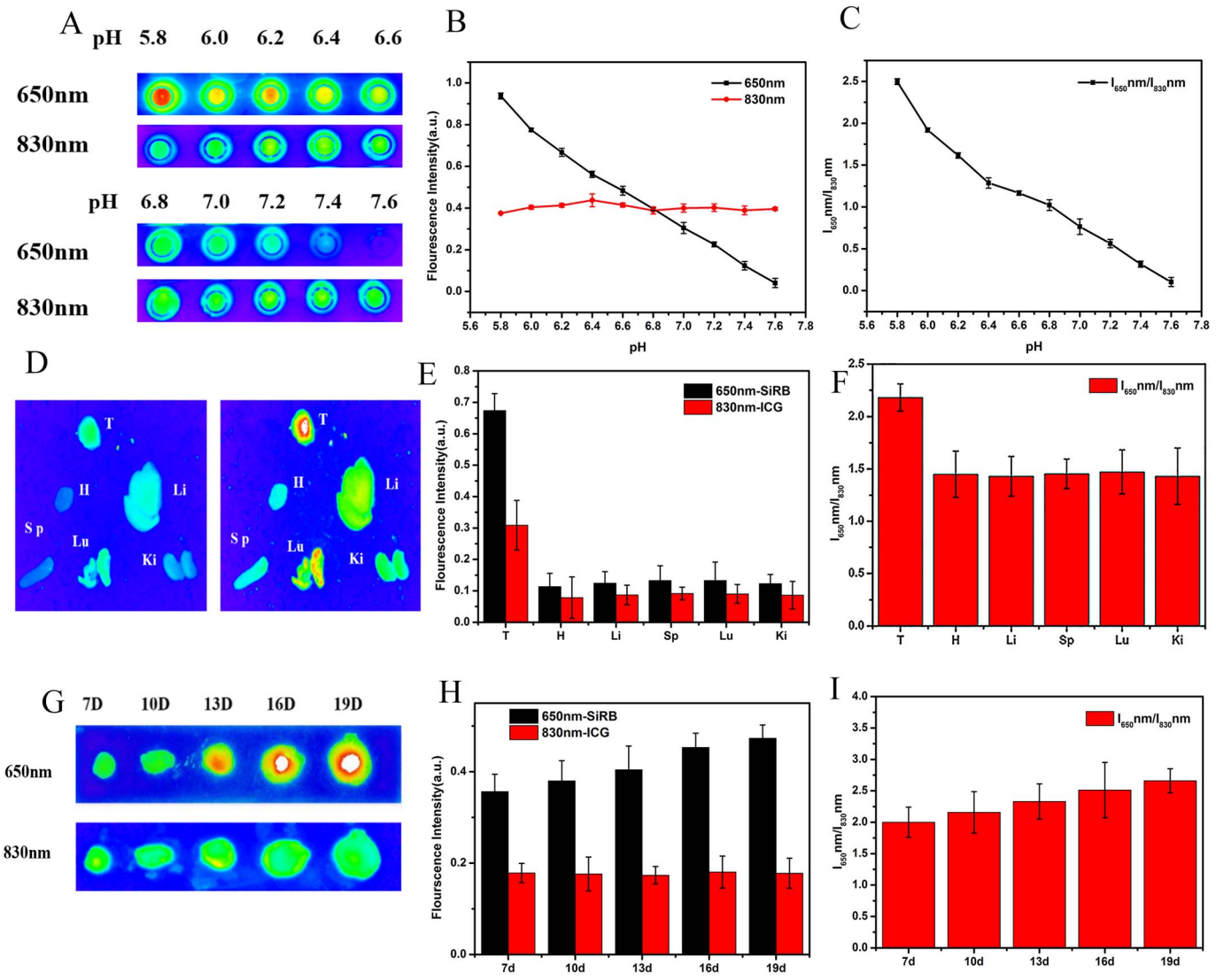

Fig. 5. The pH-responsive fluorescence imaging. (A) Fluorescence imaging of PLGA-ICG-SiRB dispersed in serum solution with different pH values; (B) fluorescence intensities of ICG and SiRB under different pH values; (C) I_{650}/I_{830} intensity ratio of PLGA-ICG-SiRB measured under different pH values; (D) ex vivo fluorescence images of major organs and tumor dissected from mice *i.v.* injected with PLGA-ICG-SiRB (24 h post-injection). Li: liver, Sp: spleen, Ki: kidney, H: heart, Lu: lung, T: tumor; (E) fluorescence intensity at 650 nm and 830 nm; (F) the I_{650}/I_{830} intensity ratio in the tumor as well as other major organs measured in (D); (G) ex vivo fluorescence images of tumor with different sizes collected from mice *i.v.* injected with PLGA-ICG-SiRB (24 h post-injection); (H) fluorescence intensity at 650 nm and 830 nm; (I) the I_{650}/I_{830} intensity ratio in the tumors measured in (G).

Therefore, the PLGA-ICG-SiRB showed strong pH-dependent absorbance. The TEM images showed that PLGA encapsulated two kinds of probes to form a core-shell structure of nanoparticles. The UV absorption spectra also showed that PLGA-ICG-SiRB had two characteristic absorption peaks of 630 nm (the peak of SiRB) and 780 nm (the peak of ICG), respectively. This result further demonstrated that both probes were successfully packed in the PLGA.

In vitro cytotoxicity studies, the cell viability of the preparation group was significantly higher than that of the free probe group, indicating that the encapsulation of PLGA reduced the cytotoxicity of the probe. Moreover, the PLGA-ICG-SiRB was still non-toxic to cells even at higher probe concentrations, which was attributed to the excellent biocompatibility of PLGA (de Groot et al., 2017). The probe release experimental results in vitro showed that PLGA can split itself in response to the slightly acidic environment, which provided the basis for the specific release of the probes (Kang et al., 2017; Santhosh et al., 2017).

In this paper, we also examined the stability of PLGA-ICG-SiRB and the effects of common salts on the fluorescence emission. The experimental results showed that the particle size of the PLGA-ICG-SiRB did not change significantly within the measured time range, indicating that the stability of the nanoparticles was superior. The addition of NaCl, KCl, $CaCl_2$ to the buffer solution did not affect the UV absorption of the PLGA-ICG-SiRB, indicating that the salts did not affect the structure of the nanoparticles and the fluorescence emission properties. Moreover, we measured their UV absorbance at different pH solution, indicating that these salts did not affect the fluorescence switch function of PLGA-ICG-SiRB.

In the laser confocal fluorescence microscope, we were surprised to find that the fluorescent probe SiRB has a good ability to enter the cell and certain lysosomal targeting effect. These results demonstrated that probe SiRB possessed great cell membrane permeability and suitability of specific labeling of acidic lysosomes in living cells. In living cells, lysosome is a major subcellular organelle that contains numerous enzymes and protein displaying a variety of activities and function at pH values (4.5–5.5). Searching for lysosome-targetable fluorescent probes is an active field as well as a challenge for the analytical chemistry research effort (Liang et al., 2018). So the probe we prepared is promising for various studies targeting lysosomes. We speculate the efficient lysosome-targeting location of SiRB without the intentionally

functionalized lysosome-locating group was attributed to the H^+-triggered ring-opening process with appropriate pK_{cycl} value that matched well with the pH value of the acidic lysosomes.

In the *vitro* fluorescence imaging experiment, we calculated the linear regression equation between the fluorescence ratio and the pH value by calculating the ratio of the two fluorescence intensities at different pH values. Since the linear regression equation has a good linearity coefficient R^2, we can calculate the corresponding pH value by substituting the fluorescence emission data into the equation. Robert and Ronald reported the methods that using magnetic resonance spectroscopy (MRS), pH-sensitive proteins and pH-sensitive MR contrast agents to measure cell and tissue pH (Robert and Ronald, 2001). We estimated the pH of the tumor site, the results were consistent with that obtained by using the method of Robert's.

Due to the auto-fluorescence of the animal and the limited penetration ability of fluorescent imaging, we first dissected the various organs of the mice, and then carried out fluorescence imaging experiments. The results showed that the pH value of the tumor site was significantly lower than that of other organs, and the concentration of nanoparticles in the tumor site was significantly higher than that of other organs. Because the fluorescence intensity of ICG does not change with the pH value, while relates with its concentration, it can be shown that PLGA-ICG-SiRB in the tumor site aggregation. The rather efficient tumor homing of the nanoparticles may be due to the enhanced permeability and retention effect. Then, we detected the pH value of the tumor with different growth days. The experimental results showed that with the growth of the tumor, the tumor microenvironment acidity will continue to increase in the measured range. This may be due to the continuous accumulation of acidic substances during the growth of the tumor leading to a decrease in the pH value of the tumor microenvironment. Based on above results, the PLGA-ICG-SiRB pH detection system will exert potential theranostic effect in future tumor diagnosis and treatment.

5. Conclusions

In conclusion, we successfully synthesized the near-infrared fluorescence probe SiRB, which has a sensitive response at pH 5.8–7.6. Based on this probe, we can prepare the PLGA-ICG-SiRB nanoparticles which can be used to accurately reflect the pH value of tumor by fluorescence ratio imaging. The PLGA-ICG-SiRB nanoparticles have dual pH sensitivity. So, after the accumulation in the tumor by EPR effect, the PLGA accelerates the cleavage to release the probes in the tumor acidic environment. SiRB is excited by H^+ to transform from the quenched state to the excited state. By the fluorescence intensity ratio changes of the PLGA-ICG-SiRB probe can accurately reflect the tumor pH values and pH changes. The applications of the PLGA-ICG-SiRB probe in tumor detection and the research on tumor microenvironment have great potential.

Supplementary data to this article can be found online at https://doi.org/10.1016/j.ejps.2018.03.015.

Acknowledgement

The authors gratefully acknowledge financial support from the Scientific and Technological Project of Henan Province of China (Grant no. 52110131).

Disclosure

The authors declare no competing financial interest.

References

Alkatout, I., Hubner, F., Wenners, A., Hedderich, J., Wiedermann, M., Sanchez, 2017. In situ localization of tumor cells associated with the epithelial-mesenchymal transition marker Snail and the prognostic impact of lymphocytes in the tumor microenvironment in invasive ductal breast cancer. Exp. Mol. Pathol. 102, 268–275.

Chen, J., Li, Y., Lv, K., Zhong, W., Wang, H., Wu, Z., 2016. Cyclam-functionalized carbon dots sensor for sensitive and selective detection of copper (II) ion and sulfide anion in aqueous media and its imaging in live cells. Sensors Actuators B Chem. 224, 298–306.

de Groot, A.M., Du, G., Mönkäre, J., Platteel, A.C., Broere, F., Bouwstra, J.A., 2017. Hollow microneedle-mediated intradermal delivery of model vaccine antigen-loaded PLGA nanoparticles elicits protective T cell-mediated immunity to an intracellular bacterium. J. Control. Release 266, 27–35.

Dervisevic, M., Senel, M., Cevik, E., 2017. Novel impedimetric dopamine biosensor based on boronic acid functional polythiophene modified electrodes. Mater. Sci. Eng., C 72, 641–649.

Florence, M.E., Massuda, J.Y., Soares, T.C., Stelini, R.F., Poppe, L.M., Brocker, E.B., de Souza EM, 2015. p53 immunoexpression in stepwise progression of cutaneous squamous cell carcinoma and correlation with angiogenesis and cellular proliferation. Pathol. Res. Pract. 211, 782–788.

Gandellini, P., Andriani, F., Merlino, G., D'Aiuto, F., Roz, L., Callari, M., 2015. Complexity in the tumour microenvironment: Cancer associated fibroblast gene expression patterns identify both common and unique features of tumour-stroma crosstalk across cancer types. Semin. Cancer Biol. 35, 96–106.

Gu, B., Wang, Y., Burgess, D.J., 2015. In vitro and in vivo performance of dexamethasone loaded PLGA microspheres prepared using polymer blends. Int. J. Pharm. 496, 534–540.

Guimaraes, P.P., Oliveira, M.F., Gomes, A.D., Gontijo, S.M., Cortes, M.E., 2015. PLGA nanofibers improve the antitumoral effect of daunorubicin. Biointerfaces 136, 248–255.

H.S, G., Melavanki, R.M., D, N., P, B., Kusanur, R.A., 2017. Binding of boronic acids with sugars in aqueous solution at physiological pH - estimation of association and dissociation constants using spectroscopic method. J. Mol. Liq. 227, 37–43.

Hui, L., Chen, Y., 2015. Tumor microenvironment: sanctuary of the devil. Cancer Lett. 368, 7–13.

Joyce, J.A., 2005. Therapeutic targeting of the tumor microenvironment. Cancer cell 7, 513–520.

Kanamala, M., Wilson, W.R., Yang, M., Palmer, B.D., Wu, Z., 2016. Mechanisms and biomaterials in pH-responsive tumour targeted drug delivery: a review. Biomaterials 85, 152–167.

Kang, B.S., Choi, J.S., Lee, S.E., Lee, J.K., Kim, T.H., Jang, W.S., 2017. Enhancing the in vitro anticancer activity of albendazole incorporated into chitosan-coated PLGA nanoparticles. Carbohydr. Polym. 159, 39–47.

Kim, T.I., Jeong, K.H., Shin, M.K., 2015. Verrucous epidermal nevus (VEN) successfully treated with indocyanine green (ICG) photodynamic therapy (PDT). JAAD Case Rep. 1, 312–314.

Lau, J.T., Lo, P.C., Jiang, X.J., Wang, Q., Ng, D.K., 2014. A dual activatable photosensitizer toward targeted photodynamic therapy. J. Med. Chem. 57, 4088–4097.

Li, B., Gb, Ge, Wen, L., Yuan, Y., Zhang, R., Peng, X., 2017. A lysosomal probe for monitoring of pH in living cells and ovarian tumour. Dyes Pigments 139, 318–325.

Liang, B., Wang, B., Ma, Q., Xie, C., Li, X., Wang, S., 2018. A lysosome-targetable turn-on fluorescent probe for the detection of thiols in living cells based on a 1,8-naphthalimide derivative. Spectrochim. Acta, Part A 192, 67–74.

Lukinavicius, G., Umezawa, K., Olivier, N., Honigmann, A., Yang, G., 2013. A near-infrared fluorophore for live-cell super-resolution microscopy of cellular proteins. Nat. Chem. 5, 132–139.

Robert, J.G., Ronald, M.L., 2001. Frontiers in the measurement of cell and tissue pH. Novartis Found. Symp. 240, 7–22.

Ruhm, A., Gobel, W., Sroka, R., Stepp, H., 2014. ICG-assisted blood vessel detection during stereotactic neurosurgery: simulation study on excitation power limitations due to thermal effects in human brain tissue. Photodiagn. Photodyn. Ther. 11, 307–318.

Santhosh, K.T., Alizadeh, A., Karimi-Abdolrezaee, S., 2017. Design and optimization of PLGA microparticles for controlled and local delivery of Neuregulin-1 in traumatic spinal cord injury. J. Control. Release 261, 147–162.

Tao, J., Wang, X.C., Chen, X.Q., Li, T.C., Diao, Q.P., Yu, H.F., 2017. Si-rhodamine B thiolactone: a simple long wavelength operating chemosensor for direct visual recognition of Hg^{2+}. Dyes Pigments 137, 601–607.

Uno, S.N., Kamiya, M., Yoshihara, T., Sugawara, K., Okabe, K., Tarhan, M.C., 2014. A spontaneously blinking fluorophore based on intramolecular spirocyclization for live-cell super-resolution imaging. Nat. Chem. 6, 681–689.

Wang, T., Zhao, Q.J., Hu, H.G., Yu, S.C., Liu, X., Liu, L., 2012. Spirolactonized Si-rhodamine: a novel NIR fluorophore utilized as a platform to construct Si-rhodamine-based probes. Chem. Commun. 48, 8781–8783.

Wang, H., Zhang, P., Hong, Y., Zhao, B., Yi, P., Chen, J., 2017. Ratiometric imaging of lysosomal hypochlorous acid enabled by FRET-based polymer dots. Polym. Chem. 8, 5795–5802.

Wu, T., Dai, Y., 2017. Tumor microenvironment and therapeutic response. Cancer Lett. 387, 61–68.

Yan, M., Jurasz, P., 2016. The role of platelets in the tumor microenvironment: from solid tumors to leukemia. Biochim. Biophys. Acta 1863, 392–400.

Yang, F., Yu, Y., 2015. Tumor microenvironment-the critical element of tumor metastasis. Chin. J. Lung Cancer 18, 48–54.

Zhao, Y., Ren, W., Zhong, T., Zhang, S., Huang, D., Guo, Y., 2016. Tumor-specific pH-responsive peptide-modified pH-sensitive liposomes containing doxorubicin for enhancing glioma targeting and anti-tumor activity. J. Control. Release 222, 56–66.

Zhu, W.W., Chai, X.Y., Wang, B.G., Zou, Y., Wang, T., Meng, Q.G., 2015. Spiroboronate Si-rhodamine as a near-infrared probe for imaging lysosomes based on the reversible ring-opening process. Chem. Commun. 51, 9608–9611.